Kelvin–Helmholtz instability in a Hele-Shaw cell: Large effect from the small region near the meniscus

E. J. Hinch[a)]
DAMTP-CMS, Cambridge CB3 OWA, United Kingdom

F. Plouraboué
DAMTP-CMS, Cambridge CB3 OWA, United Kingdom and Institut de Mécanique des Fluides de Toulouse, UMR 5502 CNRS, Toulouse, France

In an attempt to improve the poor prediction of our previous theory, we examine corrections from the small region in a Hele-Shaw cell near the meniscus where the flow is three dimensional. At larger Reynolds numbers, we find an $O(1)$ change to the effective boundary condition for mass conservation which is to be applied to the large scale flow outside the small region. © *2005 American Institute of Physics.* [DOI: 10.1063/1.1914729]

I. INTRODUCTION

The Kelvin–Helmholtz instability in a Hele-Shaw cell has been studied experimentally by Gondret and Rabaud,[1] who observed the interface between two horizontal flows of a fast gas above a slow viscous liquid. They also performed a simple stability analysis based on the Darcy equation for the gap-averaged flow in a Hele-Shaw cell with an additional term representing inertial effects, which also just used the gap-average velocity. We reexamined this problem[2] by replacing the gap-averaged description with an asymptotic analysis of the Navier–Stokes equation which exploited the thinness of the gap compared with the wavelength of the instability. The prediction of our more detailed theory was some 20% too small for the critical gas velocity at the onset of instability, whereas Gondret and Rabaud's simple theory was relatively close to their experimental observations. We observed many subtle differences between the theory and the experimental conditions, but none that we could estimate accounted for the large 20% discrepancy. This paper returns to the long-wave approximation, to find corrections from the previously neglected small region near the meniscus.

The appropriate small parameter to measure the thickness of the half gap h compared with the wavelength of the instability, $2\pi/k$, is $\epsilon = kh$, which had a value around 0.13 in the experiments. Our initial hopes were to find a correction of 2ϵ to remove the 20% shortfall in the previous predictions. Of course the long-wave approximation often has corrections $O(\epsilon^2)$ which would have been too small. To our surprise we find an $O(1)$ correction, a large effect from the small region.

Our previous calculation of the large-scale flows away from the meniscus now becomes the outer approximation in a matched asymptotic expansion in which the inner approximation is the flow in the small region near to the meniscus. Our previous calculation applied an intuitive boundary condition of the conservation of mass flux on the outer flows above and below the neglected meniscus region. Matching the asymptotic expansions, we now find $O(1)$ changes to that intuitive boundary condition, because hidden in the meniscus there is a large and varying mass flux along the interface.

In this paper we restrict attention to the critical gas velocity at the onset of the Kelvin–Helmholtz instability. We shall not study the associated phase velocity of the instability, which involves awkward questions of how the contact line moves. Fortunately, the calculation of the real and imaginary parts of the wave velocity decouple in this linear stability analysis.

The details of the three-dimensional flow in the small region near the meniscus require numerical solution. To simplify the numerical problem, we make a gross simplification of the geometry by assuming 90° contact angles of the liquid–gas interface with the side walls, so making the interface nearly flat across the gap. This unjustified simplification will mean that we cannot make detailed comparison with the experiments, but instead can only indicate that there is a significant effect to be taken into account.

II. GOVERNING EQUATIONS

A. Gas–liquid decoupling

We will solve the Navier–Stokes equations in each fluid

$$\boldsymbol{\nabla} \cdot \mathbf{u} = 0,$$

$$\rho \frac{D\mathbf{u}}{Dt} = -\boldsymbol{\nabla} p + \mu \nabla^2 \mathbf{u} + \rho \mathbf{g},$$

using subscripts g and l for the gas and the liquid, initially in $z > 0$ and $z < 0$, respectively. We apply no-slip boundary conditions on the vertical sidewalls

$$\mathbf{u} = \mathbf{0} \quad \text{on } y = \pm h.$$

On the disturbed interface between the gas and the liquid $z = \zeta'(x, y, t)$, which will satisfy

---

[a)]Author to whom correspondence should be addressed. Electronic mail: ejh1@damtp.cam.ac.uk

$$\frac{\partial \zeta'}{\partial t} + \mathbf{u} \cdot \boldsymbol{\nabla} \zeta' = w,$$

we apply continuity of velocity and a jump in the stress due to capillary pressure

$$[\sigma \cdot \mathbf{n}] = -\gamma \kappa \mathbf{n},$$

where κ is the surface mean curvature and γ the surface tension.

The viscosity of the liquid is very much larger than that of the gas, $\mu_l \gg \mu_g$, and this permits a useful decoupling of the calculation of the flow in the gas and the liquid.[2] Because the length scales of the flow and viscous stresses are similar in the gas and the liquid, the velocities in the gas must be very much larger than those in the liquid, by a factor μ_l / μ_g. Hence as far as the fast gas is concerned, the liquid is virtually stationary. This means when calculating the gas flow we may treat the surface perturbation as static and may apply there a no-slip boundary condition

$$\mathbf{u}_g = \mathbf{0} \quad \text{on } z = \zeta'.$$

Once the decoupled gas flow is found, we may calculate the viscous stress it exerts on the liquid,

$$\sigma_l \cdot \mathbf{n} = \sigma_g \cdot \mathbf{n} + \gamma \kappa \mathbf{n}.$$

This stress then drives the flow in the liquid. Solving this decoupled flow in the liquid, we eventually find its velocity at the interface. The component of the liquid velocity at the surface which is in phase with the surface perturbation is responsible for the growth of the disturbance, while the out-of-phase component produces a propagation of the disturbance. In this paper we aim to find the onset conditions, i.e., the conditions under which the in-phase component of the velocity of the liquid at the interface vanishes.

There are two stabilizing mechanisms of the Kelvin–Helmholtz instability, gravity and surface tension, both acting on the length scale of a wavelength. Disturbances to the interface on the smaller length scale of the gap between the plates could therefore produce very large capillary pressures which cannot be sustained. Hence the disturbance of the interface across the gap must have a very small amplitude, which can therefore be achieved very rapidly. Hence the cross-sectional shape adopts, quasi-instantaneously and by very small displacements, a shape consistent with the given contact angles which gives no velocity at the interface that could distort the shape, leaving just a single net mass-flow mode.

B. Mean flow

Before we look at the instability, we need to find the base or mean flow when the interface is flat, $\zeta \equiv 0$. The mean flow is driven by a constant horizontal pressure gradient, which by continuity in normal stress must be identical in the gas and the liquid,

$$\frac{d\bar{p}_g}{dx} = \frac{d\bar{p}_l}{dx}.$$

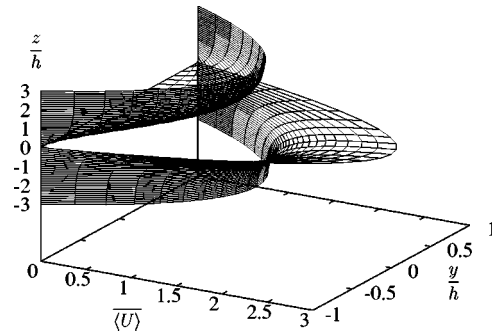The unidirectional flows $\bar{\mathbf{u}} = [\bar{u}(y,z),0,0]$ satisfy

FIG. 1. The mean velocity in the gas $z > 0$ and in the liquid $z < 0$ normalized by their different gap-averaged values far from the interface, $\langle U_g \rangle$ and $\langle U_l \rangle$, which differ by a factor μ_l / μ_g.

$$0 = -\frac{d\bar{p}}{dx} + \mu \left(\frac{\partial^2 \bar{u}}{\partial y^2} + \frac{\partial^2 \bar{u}}{\partial z^2} \right).$$

Far from the interface, the mean flow becomes parabolic

$$\bar{u} \rightarrow -\frac{1}{2\mu} \frac{d\bar{p}}{dx} (h^2 - y^2) \quad \text{as } z \rightarrow \pm \infty.$$

In the gas, we need to add to this far-field a harmonic function which enables the no-slip boundary condition to be satisfied on the interface $z = 0$. Thus

$$\bar{u}_g = \frac{3}{2} \langle U_g \rangle \left(1 - \frac{y^2}{h^2} \right)$$
$$- \langle U_g \rangle \sum_{n=0} \frac{48(-)^n}{\pi^3 (2n+1)^3} \cos \left(\frac{(2n+1)\pi y}{2h} \right) e^{-(2n+1)\pi z/2h},$$

where the gap-averaged mean flow is

$$\langle U_g \rangle = -\frac{h^2}{3\mu_g} \frac{dp_g}{dx}.$$

Figure 1 shows that the mean flow achieves the far-field parabolic form very rapidly, well within 1% by $z > 2h$.

The mean flow in the liquid is driven by the pressure gradient as well as a viscous stress applied by the above gas flow, i.e.,

$$\mu_l \frac{\partial \bar{u}_l}{\partial z} = \mu_g \frac{\partial \bar{u}_g}{\partial z} \quad \text{on } z = 0.$$

One can easily verify that the liquid mean flow is given by

$$\bar{u}_l(y,z) = \frac{\mu_g}{\mu_l} [2\bar{u}_g(y,\infty) - \bar{u}_g(y,-z)].$$

Again the mean flow achieves its far-field form very rapidly. The flow of the liquid at the interface is exactly twice the far-field parabola, one half being pushed along by the pressure gradient and the other half being pulled along by the tangential viscous stress from the gas.

C. Linearized perturbation

We now linearize the governing equations for a small disturbance $\mathbf{u}'$ of the base flow $\bar{\mathbf{u}}$. This linearization requires a small displacement of the interface $\zeta' \ll h$ and a small slope $\partial \zeta' / \partial x \ll 1$. The linearized Navier–Stokes equations are

$$\boldsymbol{\nabla} \cdot \mathbf{u}' = 0,$$

$$\rho \left(\frac{\partial \mathbf{u}'}{\partial t} + \bar{u} \frac{\partial \mathbf{u}'}{\partial x} + \mathbf{u}' \cdot \boldsymbol{\nabla} \bar{\mathbf{u}} \right) = - \boldsymbol{\nabla} p' + \mu \nabla^2 \mathbf{u}'.$$

No-slip boundary conditions must be applied on the sidewalls.

Linearizing the boundary condition that the gas velocity vanishes on the disturbed interface, we have

$$\left(\zeta' \frac{\partial \bar{u}_g}{\partial z}, 0, 0 \right) + \mathbf{u}'_g = 0 \quad \text{at } z = 0.$$

All the perturbed flow in the gas is driven by the first term in expression above, the nonvanishing mean gas flow on the perturbed interface.

Similarly linearizing the stress boundary condition, we have

$$\zeta' \bar{\sigma}_z \cdot \bar{\mathbf{n}} + \sigma' \cdot \bar{\mathbf{n}} + \bar{\sigma} \cdot \mathbf{n}'$$

$$= (\zeta' \mu \bar{u}_{zz}, 0, - \zeta' \bar{p}_z)$$

$$+ (\mu(u'_z + w'_x), \mu(v'_z + w'_y), - p' + 2\mu w'_z)$$

$$+ (\bar{p} \zeta'_x - \mu \bar{u}_y \zeta'_y, \bar{p} \zeta'_y - \mu \bar{u}_y \zeta'_x, - \mu \bar{u}_z \zeta'_x)$$

evaluated at $z = 0$ must jump by the capillary pressure $[0, 0, \gamma(\zeta'_{xx} + \zeta'_{yy})]$. In the expression for the surface curvature, we have assumed that the interface is nearly flat, as appropriate for the 90° contact angle. Now in the gas, $\bar{p}_{gz} = - \rho_g g$, which is negligibly small compared with the similar term in the liquid. Moreover on the interface $z = 0$, $\bar{u}_g = 0 = w'_g$ for all y and x, and so several terms vanish, $w'_{gx} = w'_{gy} = \bar{u}_{gy} = 0$. Also from our expression for the mean flow in the liquid, we have $\mu_l \bar{u}_{lzz} = - \mu_g \bar{u}_{gzz}$ on $z = 0$, as well as $\mu_l \bar{u}_{lz} = \mu_g \bar{u}_{gz}$. Finally, the pressure in the mean flow $\bar{p}$ is continuous at $z = 0$. Hence the viscous stresses exerted by the gas on the liquid on $z = 0$ are

$$\mu_l(u'_{lz} + w'_{lx}) - \mu_l \bar{u}_{ly} \zeta'_y = 2\zeta' \mu_g \bar{u}_{gzz} + \mu_g u'_{gz},$$

$$\mu_l(v'_{lz} + w'_{ly}) - \mu_l \bar{u}_{ly} \zeta'_x = \mu_g v'_{gz},$$

$$\zeta' \rho_l g - p'_l + 2\mu_l w'_{lz} = - p'_g + 2\mu_g w'_{gz} + \gamma(\zeta'_{xx} + \zeta'_{yy}). \quad (1)$$

The liquid flow evaluated at the interface $z = 0$ gives by the kinematic boundary condition the slow evolution of the surface disturbance

$$\frac{\partial \zeta'}{\partial t} + \bar{u}_l \frac{\partial \zeta'}{\partial x} = w_l \quad \text{at } z = 0.$$

We will now consider a perturbation of the interface with a real wavenumber k and complex velocity c whose imaginary part will give the growth rate and real part the speed of propagation. Thus

$$\zeta'(x, y, t) = \zeta_0 e^{ik(x-ct)} [1 + \epsilon^3 \zeta''(y)].$$

Here we take ζ_0 to be the gap-averaged perturbation. The variation of the interface across the gap, $\zeta''(y)$, is required to drive a redistribution of the vertical velocity of the liquid at the interface which enables the kinematic boundary condition above to be satisfied with the parabolic $\bar{u}_l$ and ζ' constant (to leading order). We shall find that this variation of the interface across that gap is very small, $O(\epsilon^3)$.

III. GAS FLOW

A. Nondimensionalization

As we must concentrate our attention on the small meniscus region, we scale the flow direction x by the inverse wavenumber k^{-1} and the cross-gap direction y and vertical direction z by the gap half separation h. The mean flow $\bar{u}_g$ is scaled by its gap-averaged value far from the interface $\langle U_g \rangle$. The x component of the velocity perturbation u' is scaled by $\langle U_g \rangle \zeta_0 / h$, which is the scale of the mean flow at a height $z = \zeta_0$. The other two components of the velocity perturbation, v' and w', are scaled by $\langle U_g \rangle k \zeta_0$, which is the mean flow times the slope of the perturbed interface. Note that in common with boundary-layer problems the cross-gap and vertical velocity perturbations are smaller than that in the downstream direction by the small factor kh. Finally the pressure perturbation is scaled viscously by $\mu_g \langle U_g \rangle \zeta_0 / h^2$.

Dropping the primes on the perturbation quantities, and remembering that the gas problem is quasistatic, the nondimensionalized equations governing the gas flow are

$$u_{gx} + v_{gy} + w_{gz} = 0,$$

$$\text{Re}(\bar{u}_g u_{gx} + v_g \bar{u}_{gy} + w_g \bar{u}_{gz}) = - \epsilon p_{gx} + \epsilon^2 u_{gxx} + \nabla_2^2 u_g,$$

$$\text{Re} \, \bar{u}_g v_{gx} = - \epsilon^{-1} p_{gy} + \epsilon^2 v_{gxx} + \nabla_2^2 v_g,$$

$$\text{Re} \, \bar{u}_g w_{gx} = - \epsilon^{-1} p_{gz} + \epsilon^2 w_{gxx} + \nabla_2^2 w_g, \quad (2)$$

where

$$\nabla_2^2 = \frac{\partial^2}{\partial y^2} + \frac{\partial^2}{\partial z^2}, \quad \text{Re} = \rho_g \langle U_g \rangle k h^2 / \mu_g$$

is the reduced Reynolds number comparing advection along the streamlines with viscous diffusion across streamlines, and

$$\epsilon = kh$$

is the small parameter measuring the thickness of the gap relative to the wavelength of the instability. The boundary conditions to be satisfied are

$$u_g = v_g = w_g = 0 \quad \text{on } y = \pm 1,$$

$$u_g + \zeta \bar{u}_{gz} = v_g = w_g = 0 \quad \text{on } z = 0,$$

where the nondimensionalized quasistatic interface perturbation becomes

$$\zeta = e^{ix}(1 + \epsilon^3 \zeta'').$$

B. Inner expansion for the meniscus region

The governing equations above have the standard feature of boundary-layer equations that the pressure must be constant at leading order across the inner region, otherwise there would be large sideways accelerations for v_g and w_g. This feature follows from the different scalings of the different velocity components. Thus we seek an expansion in small ϵ,

$$p_g(x,y,z,t) \sim e^{ix}[p_{g0} + \epsilon p_{g1}(y,z)],$$

$$\mathbf{u}_g(x,y,z,t) \sim e^{ix}\mathbf{u}_{g0}(y,z).$$

The governing equations then become, at leading order,

$$iu_{g0} + v_{g0y} + w_{g0z} = 0, \tag{3}$$

$$\mathrm{Re}(i\bar{u}_g u_{g0} + v_{g0}\bar{u}_{gy} + w_{g0}\bar{u}_{gz}) = \nabla_2^2 u_{g0},$$

$$\mathrm{Re}\, i\bar{u}_g v_{g0} = -p_{g1y} + \nabla_2^2 v_{g0},$$

$$\mathrm{Re}\, i\bar{u}_g w_{g0} = -p_{g1z} + \nabla_2^2 w_{g0}, \tag{4}$$

with boundary conditions

$$u_{g0} = v_{g0} = w_{g0} = 0 \quad \text{on } y = \pm 1,$$

$$u_{g0} = -\bar{u}_{gz}, \quad v_{g0} = w_{g0} = 0 \quad \text{on } z = 0. \tag{5}$$

There is also a matching condition to the outer flow as $z \to \infty$.

The inner-region gas flow is driven by the boundary condition $u_{g0} = -\bar{u}_{gz}$ on $z=0$. The u component of the flow is controlled by the u-momentum equation. The v and w components of velocity are then required to be nonzero in order to satisfy the mass conservation: they are forced by the transverse pressure gradient from p_{g1}. In normal one-dimensional boundary layers there is no need for such transverse pressure gradients, but in the inner region here the transverse velocities must vary over the short distance of the gap in order to satisfy their boundary conditions.

C. Outer flow

The flow in the outer region is that we calculated earlier.[2] Far from the meniscus, as $z \to \infty$, the mean flow assumes its (nondimensional) parabolic form

$$\bar{u}_g \to \frac{3}{2}(1 - y^2).$$

The cross-gap flow v_g vanishes in the outer region, while the vertical and downstream components become of similar dimensional size. This requires a rescaling of our nondimensional velocities

$$u_g = \epsilon U_g.$$

Similarly the length scale for variations in the vertical direction is no longer the gap thickness but the wavelength, requiring a rescaling

$$z = \epsilon^{-1}Z.$$

With these rescalings, the governing equations become at leading order

$$U_{gx} + w_{gZ} = 0,$$

$$\mathrm{Re}\,\bar{u}_g U_{gx} = -p_{gx} + U_{gyy},$$

$$\mathrm{Re}\,\bar{u}_g w_{gx} = -p_{gZ} + w_{gyy},$$

with corrections $O(\epsilon^2)$.

The solution of these outer equations has the following potential form (accurate to all orders in ϵ^n),

$$p_g(x,Z) = Q_g P e^{ix-Z},$$

$$U_g(x,y,Z) = Q_g e^{ix-Z}f(y),$$

$$w_g(x,y,Z) = Q_g i e^{ix-Z}f(y),$$

where Q_g is a matching constant to be determined. The velocity profile $f(y)$ satisfies

$$\mathrm{Re}\, i\frac{3}{2}(1 - y^2)f = -iP + f'' \quad \text{in } -1 < y < 1,$$

with boundary conditions

$$f = 0 \quad \text{on } y = \pm 1,$$

and with normalization constant P given by

$$\int_{-1}^{1} f\, dy = 2.$$

This normalization gives the velocity profile unit mass flux, corresponding to the outer flow responding exactly to the kinematic movement of the interface without an intervening inner region. The matching constant Q_g can therefore be viewed as the effect on the mass flux produced by the inner region.

Results for the velocity profile $f(y)$ at various Reynolds numbers Re were reported earlier,[2] where we also gave results for the normalization constant $P(\mathrm{Re})$. Due to a different nondimensionalization of the pressure, a viscous scaling in this paper compared with an inertial scaling before, the values of P in this paper are Re times the values reported earlier.

D. Matching

Re-expressing the above outer solution in terms of the inner variables and taking the limit $\epsilon \to 0$, which forces $Z \to 0$, gives the matching conditions on the inner solution as $z \to \infty$

$$u_{g0} \to 0, \quad v_{g0} \to 0, \quad w_{g0} \to Q_g i f(y),$$

$$p_{g0} = Q_g P, \quad p_{g1} \to -Q_g P z + Q_{g1}P, \tag{6}$$

where Q_{g1} is a small ϵ correction to the leading order matching constant Q_g.

We first note that unlike standard boundary-layer problems the leading-order downstream velocity u_{g0} decays out of the inner region. This is necessary if the downstream component is to become the same size as the vertical component in the outer region.

The interplay between the inner and outer regions of the gas flow can now be understood. The inner flow is driven by the boundary condition $u_{g0} = -\bar{u}_{gz}$ on $z=0$, and through the mass conservation produces a vertical flow $w_{g0} = Q_g i f(y)$ out of the inner region. The outer flow responds to this mass flux Q_g out of the inner region, producing a pressure $Q_g P$ on the inner region, which passes straight through the inner region as the constant p_{g0} to apply a pressure on the liquid below. This pressure will drive a flow in the liquid which in turn will move the interface.

The important matching constant Q_g is the net mass flux out of the inner region. This can be found by integrating the mass conservation equation (3) in the inner region over the width of the gap $-1 < y < 1$ and through the depth of the inner region to some large height $0 < z < H$. Thus

$$\int_{-1}^{1} dy \int_{0}^{H} dz (iu_{g0} + v_{g0y} + w_{g0z}) = 0.$$

Now the v_{g0y} term integrates across the gap between vanishing boundary conditions on the sidewalls, while the w_{g0z} term integrates vertically from vanishing boundary condition at $z=0$ to the outer form $w_{g0} \to Q_g i f(y)$, where the profile $f(y)$ integrates across the gap by normalization to 2. Hence

$$Q_g = -\frac{1}{2} \int_{-1}^{1} dy \int_{0}^{\infty} dz\, u_{g0}. \tag{7}$$

In our previous paper, we ignored the small meniscus region in the gas and assumed that the outer gas flow moved up with the interface, i.e., we assumed the mass conservation boundary condition gave $Q_g = 1$. We shall find that $Q_g = 1$ only at Re=0.

IV. LIQUID FLOW

A. Nondimensionalization

The formulation of the flow in the liquid follows closely that for the gas. The nondimensionalization of the length scales in the inner region are the same, while for the velocities the gap-averaged mean liquid velocity $\langle U_l \rangle$ replaces that for the gas, $\langle U_g \rangle$. The viscous scaling of the pressure in the liquid $\mu_l \langle U_l \rangle \zeta_0 / h^2$ is identical to that in the gas because $\mu_l \langle U_l \rangle = \mu_g \langle U_g \rangle$. With the slower velocities in the liquid, the interface is now seen to propagate, at a complex velocity c which is scaled by the gap-averaged mean liquid velocity $\langle U_l \rangle$.

The resulting nondimensionalized equations governing the liquid flow are then the same as those for the gas (2) except all the inertial terms are set to zero, because the Reynolds number for the liquid is very small, $\rho_l \mu_g^2 / \rho_g \mu_l^2$ smaller than in the gas. The no-slip boundary conditions on the sidewalls are unchanged by the nondimensionalization. The stress boundary conditions on the interface (1) take the nondimensional form

$$u_{lz} + \epsilon^2 w_{lx} = 2e^{i(x-ct)}\bar{u}_{gzz} + u_{gz},$$

$$v_{lz} + w_{ly} - \bar{u}_{ly} i e^{i(x-ct)} = v_{gz},$$

$$\text{Re}\,\Pi e^{i(x-ct)} - p_l + 2\epsilon w_{lz} = -p_g + 2\epsilon w_{gz} + \epsilon G \zeta_{yy}'' e^{i(x-ct)}$$

plus some $O(\epsilon^3)$ terms not exhibited, where

$$\Pi = (\rho_g g/k + \gamma k)/\rho_g \langle U_g \rangle^2$$

is the ratio of the stabilizing gravitational and capillary pressures to the destabilizing Bernoulli suction and another parameter

$$G = \gamma k^2 h^2 / \mu_g \langle U_g \rangle$$

which is necessarily $O(\text{Re}\,\Pi)$.

B. Inner expansion

With a similar expansion in small ϵ as employed in the gas inner meniscus region,

$$p_l(x,y,z,t) \sim e^{i(x-ct)}[p_{l0} + \epsilon p_{l1}(y,z)],$$

$$\mathbf{u}_l(x,y,z,t) \sim e^{i(x-ct)}\mathbf{u}_{l0}(y,z),$$

the governing equations at leading order then become

$$iu_{l0} + v_{l0y} + w_{l0z} = 0, \tag{8}$$

$$0 = \nabla_2^2 u_{l0},$$

$$0 = -p_{l1y} + \nabla_2^2 v_{l0},$$

$$0 = -p_{l1z} + \nabla_2^2 w_{l0}, \tag{9}$$

with boundary conditions

$$u_{l0} = v_{l0} = w_{l0} = 0 \quad \text{on } y = \pm 1, \tag{10}$$

and on $z=0$

$$u_{l0z} = 2\bar{u}_{gzz} + u_{g0z},$$

$$v_{l0z} + w_{l0y} - \bar{u}_{ly} i = v_{g0z},$$

$$\text{Re}\,\Pi - p_{l0} = -p_{g0},$$

$$-p_{l1} + 2w_{l0z} = -p_{g1} + 2w_{g0z} + G\zeta_{yy}''. \tag{11}$$

There is also a matching condition to the outer flow as $z \to -\infty$.

Finally the complex wave speed c is given by the kinematic boundary condition on $z=0$,

$$i[\bar{u}_l(y,0) - c] = w_{l0}(y,0). \tag{12}$$

This must be satisfied at each position across the gap, $-1 < y < 1$. This is made possible by the redistribution of the w_{l0} flow driven by the small variation of the shape across the gap $\zeta''(y)$. It is the need for ζ'' to occur in the last equation of Eq. (11) which dictated this perturbation to the flat interface was $O(\epsilon^3)$.
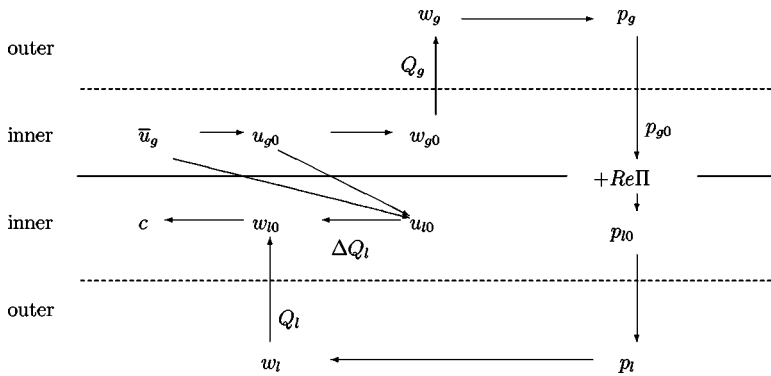
FIG. 2. Schematic representation of the matching analysis.

C. Outer flow

The outer flow in the liquid has the same rescalings as in the gas and so is governed by the same equations as for the outer flow of the gas except that the inertial terms are negligible in the liquid. Thus the solution for the outer flow in the liquid is (for all orders in ϵ^n)

$$p_l(x,Z,t) = Q_l 3 i e^{i(x-ct)+Z},$$

$$U_l(x,y,Z,t) = Q_l e^{i(x-ct)+Z} \frac{3}{2}(1-y^2),$$

$$w_l(x,y,Z,t) = -Q_l i e^{i(x-ct)+Z} \frac{3}{2}(1-y^2),$$

where Q_l is a matching constant corresponding to the mass flux in the liquid outer flow.

D. Matching

Matching the above outer flow in the liquid to the inner flow, we find that as $z \to -\infty$ the inner solution must have the following behavior:

$$u_{l0} \to 0, \quad v_{l0} \to 0, \quad w_{l0} \to -Q_l i \frac{3}{2}(1-y^2),$$

$$p_{l0} \to Q_l 3i, \quad p_{l1} \to Q_l 3iZ + Q_{l1} 3i, \tag{13}$$

where Q_{l1} is a small ϵ correction to the leading-order matching constant.

We can now see how the liquid responds to the gas. As explained in the matching of the gas flow, the outer gas flow exerts a pressure $Q_g P$ on the inner gas flow, which passes straight through the gas inner region as the constant pressure $p_{g0} = Q_g P$. This pressure is applied to the interface. After adding the stabilizing effects of gravity and surface tension in Re Π, the pressure available to drive the liquid flow is $p_{l0} = p_{g0} + \text{Re } \Pi$. This pressure passes straight through the liquid inner region as the constant pressure p_{l0} to become the pressure driving the outer flow via $Q_l 3i = p_{l0}$. The liquid outer region responds with a flow into the inner region $w_{l0} = -Q_l i \frac{3}{2}(1-y^2)$. The net mass flow into the liquid inner region is therefore $Q_l = -i(Q_g P + \text{Re } \Pi)/3$.

In order to obtain a simple expression for the complex wave velocity c, we now repeat the trick at the end of the section on matching the gas flow. We integrate the mass con-

servation equation (8) over the width of the gap $-1 < y < 1$ and through the depth of the liquid inner region $-H < z < 0$. Thus

$$\int_{-1}^{1} dy \int_{-H}^{0} dz (iu_{l0} + v_{l0y} + w_{l0z}) = 0.$$

The velocity v_{l0y} term integrates again between vanishing boundary conditions on the sidewalls, while the w_{l0z} term integrates from the input from the outer to the vertical flow on the interface,

$$-2i\Delta Q_l + \int_{-1}^{1} dy \, w_{l0}(y,0) + 2Q_l i = 0,$$

where

$$\Delta Q_l = -\frac{1}{2} \int_{-1}^{1} dy \int_{-\infty}^{0} dz \, u_{l0} \tag{14}$$

is the extra mass flux contributed from the liquid inner region. We now integrate the kinematic boundary condition on the liquid (12) across the width of the gap, using the result that the liquid mean flow on the interface is twice its value far from the interface,

$$2i(2-c) = \int_{-1}^{1} dy \, w_{l0}(y,0).$$

Substituting the result above from integrating the mass conservation and the result for the matching constant Q_l, we obtain an expression for the complex wave velocity

$$c = 2 - \Delta Q_l - \frac{i}{3}(Q_g P + \text{Re } \Pi). \tag{15}$$

This expression based on net mass fluxes avoids the need to find the small perturbation to the interface ζ'' that ensures the correct y dependence of w_{l0} on the interface which satisfies the kinematic boundary condition (12) at each y.

In our previous paper, we ignored the small meniscus region in the liquid. Thus we assumed $\frac{1}{2}\int_{-1}^{1} \bar{u}(y,0) \, dy = 1$ instead of its correct value of 2, and we also omitted the term ΔQ_l. We shall find that $\Delta Q_l = 1$ at Re$=0$, so that these two errors cancel when there is no inertia.

E. Structure of the problem

It is worth pausing here to review the structure of the stability calculation, see Fig. 2. Due to the viscosity of the gas being much smaller than that of the liquid, we can first solve the fast flow of the gas over an effectively stationary liquid. The liquid then moves slowly in response to the stresses exerted on it by the flowing gas. The vertical velocity of the liquid at the interface gives the complex wave speed of the perturbations.

Ensuring no-slip of the gas on the perturbed interface drives a perturbation to the downstream gas flow u_{g0} in the inner meniscus region. Conserving mass requires a vertical gas flow w_{g0} in the inner region. This leads to a mass flux Q_g of gas into the outer region. The response of the gas in the outer region requires a pressure field p_g. This pressure passes straight through the gas inner region, is reduced across the interface by $\mathrm{Re}\,\Pi$, the stabilizing effects of gravity and surface tension, passes straight through the liquid inner region to become a pressure field p_l in the liquid outer region. There it drives a viscous Hele-Shaw flow, which produces a vertical velocity w_l with a mass flux Q_l of liquid into the inner region. In the liquid inner region, there is also a downstream flow u_{l0} driven by the stress u_{g0z} from the perturbed gas flow and the stress from the mean flow on the perturbed interface $\bar{u}_{zz}$. A divergence in this downstream flow in the liquid inner produces the extra mass flux ΔQ_l which must be added to the mass flux Q_l entering the inner region to give the vertical velocity $w_{l0}(y,0)$ on the interface, and hence the complex wave speed c.

V. NUMERICAL SOLUTION

The problem has now been reduced to calculating the complex wave velocity c using Eq. (15), in which there appears the mass flux from the gas inner region Q_g given by integral (7), the extra mass flux from the liquid inner region ΔQ_l given by integral (14), and the pressure normalization constant $P(\mathrm{Re})$ given by our previous study[2] of the gas outer region. To evaluate the two integrals, we need to find the gas and liquid inner flows u_{g0} and u_{l0}, by solving Eqs. (3), (4), (8), and (9) with associated boundary conditions (5), (10), and (11) and matching conditions (6) and (13). These equations require numerical solution, except when the remaining parameter, the reduced Reynolds number Re, is small. We shall later give the simple solution for small Reynolds number, which yields a test of the numerical method.

A. Method

The difficulty for a numerical approach is that the flows are driven by the boundary conditions, $u_{g0}=-\bar{u}_{gz}$ on $z=0$ for the gas and $u_{l0z}=2\bar{u}_{gzz}+u_{g0z}$ on $z=0$ for the liquid. Moreover, the cross-gap and vertical components of the velocity in the gas, v_{g0} and w_{g0}, are driven by the mass conservation equation (3). Boundary conditions and mass conservation are often treated less precisely by standard numerical methods.

A finite difference method is employed. Having made the gross simplification of 90° contact angles, an equispaced Cartesian grid can be employed with

$$y = i\Delta \quad \text{for } i = -ny \text{ to } ny, \quad z = j\Delta \quad \text{for } j = -nz \text{ to } nz,$$

where $\Delta = 1/ny$ and typically $nz = 3ny$. The variables are held on a staggered grid in order to produce a compact pressure molecule without spurious pressure modes, i.e.,

$$\bar{u}_g, \bar{u}_l \quad \text{at } i\Delta, j\Delta,$$

$$v_{g0}, v_{l0} \quad \text{at } i\Delta, \left(j + \frac{1}{2}\right)\Delta,$$

$$w_{g0}, w_{l0} \quad \text{at } \left(i + \frac{1}{2}\right)\Delta, j\Delta,$$

$$u_{g0}, u_{l0}, p_{g1}, p_{l1} \quad \text{at } \left(i + \frac{1}{2}\right)\Delta, \left(j + \frac{1}{2}\right)\Delta.$$

The normal components of velocity to any boundary are therefore held on the boundary, as is the mean flow, while the tangential velocity perturbations are held half a grid-block away from the boundary. The momentum equations are satisfied for each component of velocity at the staggered point where that component is stored, using second-order central differencing of derivatives and second-order interpolation of variables held on different staggers. Boundary conditions are applied with second-order accuracy by extrapolation onto the boundary with up to three interior points as required, along with interpolation of other variables. Far-field conditions of no change in value between the boundary and one grid-block inside are applied to each component of velocity.

Mass conservation is achieved exactly, not just to second-order accuracy, by a pressure-projection method. In retrospect, a pressure-update method would have been better. The mass conservation equations are satisfied at each pressure node and then the velocity components v_0 and w_0 updated. In order to satisfy exactly the mass conservation at the next-to-boundary points while not disturbing the normal velocity component on the boundary, it was found necessary to precompensate the boundary velocity for the postprojection addition, the latter being of course the pressure boundary condition (obtained to second order by suitable extrapolation onto the boundary).

The steady solution of the system of equations was found by a time-like relaxation. First the mean flows $\bar{u}$ were relaxed to equilibrium with $15ny^2$ iterations. Then the velocity perturbations u_0, v_0, and w_0 were simultaneously relaxed to equilibrium with again $15ny^2$ iterations, and for each iteration the pressure p_1 was relaxed with $4ny$ iterations of successive overrelaxation using an overrelaxation parameter between 1.6 and 1.8. This approach is therefore an ny^5 method, which severely reduces the opportunities of doubling the spatial resolution many times.

B. Checks

A number of tests were applied to the code. First, various quantities were seen to have a second-order behavior when the spatial resolution was changed through $ny = 10$, 15, 20, and 30. Second, the distance to infinity was varied through $nz = ny, 2ny, 3ny$, and $5ny$, with $3ny$ being found to be very

adequate. Third, the mean flow in the liquid was checked to obey the reflection law $\bar{u}_l(y,z)=2\bar{u}_g(y,\infty)-\bar{u}_g(y,-z)$. This is a good test for whether the stress boundary conditions are being applied to second-order accuracy. Fourth, the mass conservation was checked to be satisfied exactly.

A more demanding fifth test of the code is the behavior at small Reynolds number Re. At Re=0, the inner equations in the gas and the liquid have a solution

$$u_{g0}=-\bar{u}_{gz}, \quad v_{g0}=0, \quad w_{g0}=i\bar{u}_g,$$

$$u_{l0}=-\bar{u}_{lz}, \quad v_{l0}=0, \quad w_{l0}=i\bar{u}_l.$$

This solution represents the streamlines of the flow being displaced exactly with the interface perturbation. Further it gives zero streamwise acceleration, although there is a vertical acceleration. This means that while w_{g0} and so v_{g0} have $O(\text{Re})$ corrections, the downstream flows u_{g0} and u_{l0} have only $O(\text{Re}^2)$ corrections. The numerical solutions are found to have such a behavior.

The solution for Re=0 also provides a test of the computational accuracy, because it gives exact answers for the mass-flux integrals $Q_g=1$ and $\Delta Q_l=1$. In the table below, we give the results for Q_g and ΔQ_l for four different spatial resolutions. The results are not very good, particularly for the liquid which is more prone to errors being driven by a stress boundary conditions. Fortunately, a Δ^2-extrapolation of adjacent pairs improves the accuracy to an acceptable level of around 1%. A refined extrapolation assuming the error has an $O(\Delta^2)$ and an $O(\Delta^3)$ component, applied to adjacent triples, gives satisfactory accuracy of nearly four significant figures.

ny	Q_l	Δ^2	$\Delta^2+\Delta^3$	ΔQ_l	Δ^2	$\Delta^2+\Delta^3$
10	0.9462			0.8844		
15	0.9741	0.9964		0.9408	0.9859	
20	0.9848	0.9986	0.9997	0.9641	0.9941	0.9986
30	0.9930	0.9996	1.0001	0.9828	0.9978	0.9998

The more refined extrapolation was applied to all the results given below for these two mass-flux integrals. At larger Reynolds numbers, higher than 60, it was found necessary to use a finer grid with $ny=40$ in order to obtain good results. Note that, as a consequence of the $O(ny^5)$ CPU cost, the 1.4% accuracy obtained from extrapolation from $ny=10$ and $ny=15$ would require without extrapolation $ny>30$ taking over 36 times the CPU for $ny=15$, while the 1.4×10^{-3} accuracy obtained from extrapolation from $ny=10$, $ny=15$, and $ny=20$ would require without extrapolation $ny>101$ taking over 3330 times the CPU for $ny=20$.

Finally a sixth test of the code was available by examining the ratio of the pressure gradient far from the interface $-p_{g1z}$ to mass flux Q_g, which should be equal to the pressure normalization constant P that we found in our previous study.[2] This last test checks the behavior of the code at nonzero Reynolds numbers.

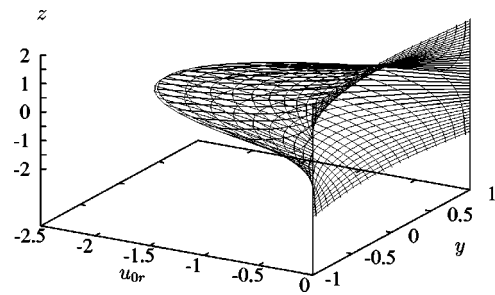

FIG. 3. The real part of the downstream velocity perturbation in the gas $z>0$ and in the liquid $z<0$ for Re=15. The nondimensionalizations of the gas and liquid velocities differ by the factor μ_l/μ_g.

VI. RESULTS

Figure 1 gives numerical results for the mean flow in the gas and in the liquid, each normalized by their gap-averaged values far from the interface. It is seen that the mean flow attains a far-field parabolic profile rapidly, with 1% by $|z|>2h$.

A. Downstream velocity u_0

The downstream perturbation velocity u_0 has real and imaginary parts. Figure 3 gives the real part at Re=15. The gas flow is driven by the boundary conditions $u_{g0}=-\bar{u}_{gz}$ on $z=0$, i.e., the gas flow must vanish on the perturbed interface. On the crests, where $\bar{u}_g>0$, one must therefore have $u_{g0}<0$, with the reverse in the troughs. Hence the real part of u_{g0}, which is the value on the crests, must be negative. This can be seen in Fig. 3.

The liquid perturbation flow u_{l0}, on the other hand, is driven by the boundary condition of the continuity of the stress on the perturbed boundary, $u_{l0z}+\bar{u}_{lzz}=u_{g0z}+\bar{u}_{gzz}$. In the gas, there is little change in the stress exerted by the gas on the perturbed interface, $u_{g0z}+\bar{u}_{gzz}\approx0$; it is $O(\text{Re}^2)$ at small Re. Now the mean velocity gradient in the liquid can be seen in Fig. 2 to increase upwards to the interface. Hence we expect a negative perturbation to the liquid viscous stress, $u_{l0z}<0$. This results in the negative velocities in the liquid seen in Fig. 3. Although Re=15 is not small, the general form of the real part of the downstream perturbation velocity u_0 is not dissimilar to the Re=0 result, $u_0=-\bar{u}_z$.

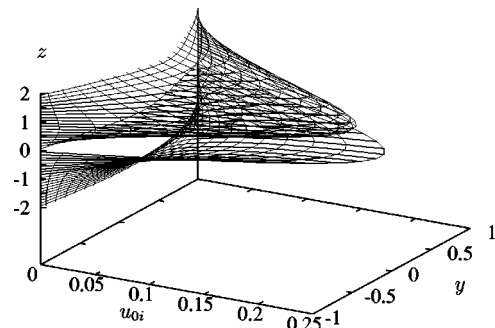The imaginary part of the downstream velocity perturbation u_0 is given in Fig. 4 at Re=15. Without inertia, the

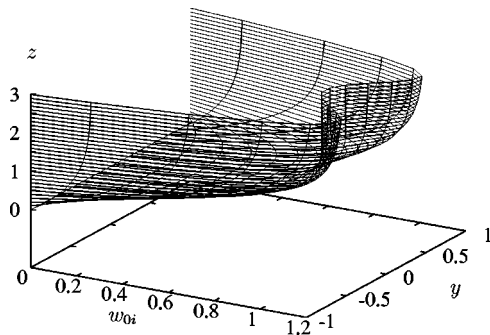FIG. 4. The imaginary part of the downstream velocity perturbation in the gas $z>0$ and in the liquid $z<0$ at Re=15.

FIG. 5. The imaginary part of the vertical velocity perturbation in the gas at Re=15.

FIG. 6. The mass flux in the gas Q_g as a function of Reynolds number Re. The continuous curves gives the real part, while the broken curve is the imaginary part.

imaginary part would vanish: at Re=15, it is small, about 10% of the real part. With a spatial variation such as e^{ix}, the imaginary part is the value at $x=-\pi/2$, i.e., a quarter wavelength before the crest, where the interface has its maximum positive slope. In the gas, the imaginary part must vanish on the boundary $z=0$. The positive value at the quarter wavelength before the crests is due to the inertia of the mean flow carrying forward the positive value in the trough before. The imaginary part of the downstream velocity in the liquid is not due to inertia in the liquid, because the liquid Reynolds number is zero. Instead this component of the liquid velocity is driven by the viscous stress exerted by the imaginary part of the gas flow, which is positive.

B. Vertical velocity w_0

Figure 5 shows the imaginary part of the vertical velocity in the gas at Re=15. The velocity vanishes at the interface and rapidly achieves the curious double-peaked form of the outer flow. This form was explained in our previous paper[2] as due to the faster advection by the mean flow on the centerline giving less time for the gap-independent pressure gradient to accelerate the flow. The imaginary part describes the flow at the quarter wavelength before the crests. A positive value of the vertical velocity corresponds to a mass-flux there out of the inner region into the outer region above. This efflux results from the convergence of the downstream velocity, which is forward in the trough behind and backwards at the crest in front. In addition to the imaginary part, there is a smaller real part from a convergence of the imaginary part of the downstream velocity. As the downstream velocity is forward on the up slope of the interface before the crest and backwards on the down slope after the crest, the real part of the vertical velocity has a small positive mass flux. The detailed profile is rather complex.

C. Mass-fluxes Q_g and ΔQ_l

From the velocity profiles described above, we can now evaluate the mass-flux integrals (7) for Q_g and (14) for ΔQ_l. The extrapolation described in Sec. V B was applied to the values of these integrals obtained from three different spatial resolutions, assuming the error had $O(\Delta^2)$ and $O(\Delta^3)$ parts. These integrals have real and imaginary parts which depend on the Reynolds number Re.
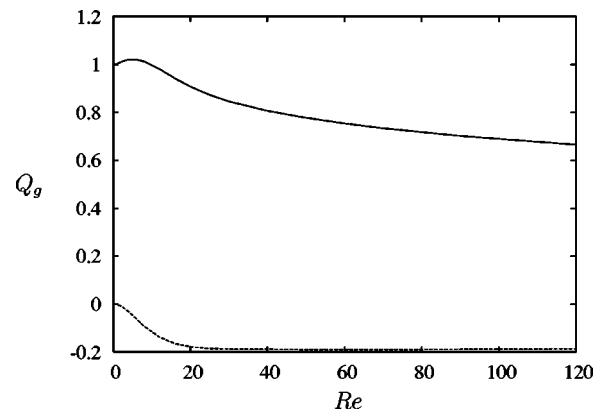
Figure 6 gives the real and imaginary parts of the gas matching constant Q_g as a function of the Reynolds number. The negative real part and positive imaginary part of u_{g0} give the mass-flux integral (7) for Q_g a positive real part and negative imaginary part. At Re=0, we have the value Q_g =1. After a small peak, the real part of Q_g decreases, falling below 0.8 by Re=40, while the imaginary part becomes negative, approaching −0.2 by Re=40. This behavior is due to advection by the mean flow. The real part of u_{g0} diffuses into $z>0$ from its value fixed by the boundary condition at $z=0$. As the fluid moves faster with stronger mean flows, it has less time to respond to this diffusion, and so the magnitude of Q_g decreases with Re. The advection also produces an out-of-phase imaginary part. There is a hint that the decrease in magnitude may be following an $Re^{-1/3}$ trend, appropriate for boundary layers in shear flows.

Figure 7 gives the real and imaginary parts of the liquid extra mass flux ΔQ_l as a function of the Reynolds number Re. As the signs of the real and imaginary part of the downstream liquid velocity u_{l0} are the same as for u_{g0} in the gas, the mass-flux integral (14) gives the same signs for the real and imaginary parts of ΔQ_l as for Q_g. At Re=0, we have the value $\Delta Q_l=1$. The liquid extra mass flux ΔQ_l has a similar
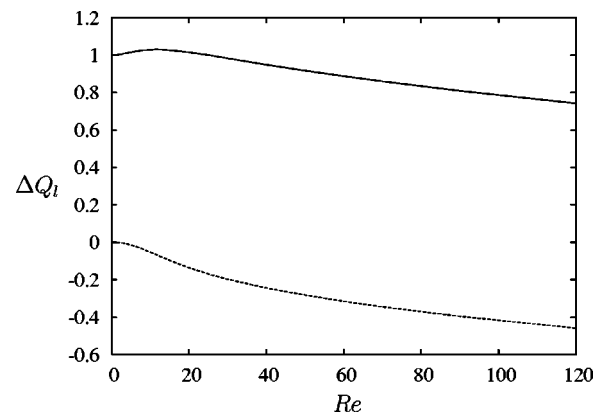

FIG. 7. The extra mass flux in the liquid ΔQ_l as a function of Reynolds number Re. The continuous curves gives the real part while the broken curve is the imaginary part.
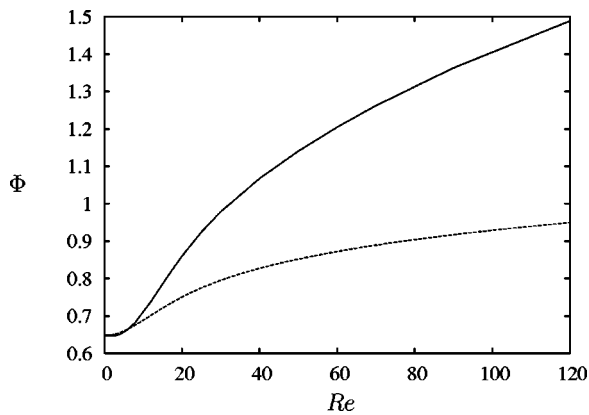
FIG. 8. The combination $\Phi(\text{Re})=\text{Re}/(-Q_{gr}P_r+Q_{gi}P_i-3\Delta Q_{li})$ representing the reduction of the critical Kelvin–Helmholtz velocity. The broken curve is the corresponding result of our first paper (Ref. 2), in which we effectively took $Q_g=1$ and $\Delta Q_l=1$.

FIG. 9. The critical gas velocity U_g scaled by V_* as a function of the wavenumber k scaled by $1/l_*$ for $\text{Re}_*=40$. The continuous curve is the result for Eq. (18). The dashed curve is the corresponding result for our previous theory (Ref. 2) for the outer ignoring the existence of the inner meniscus region. The dotted curve is for the simple Euler–Darcy theory (Ref. 1).

dependence on the Reynolds number as the gas mass flux Q_g, with the real part decaying half as much while the imaginary part decays twice as much.

D. Marginal stability

The complex wave velocity c in (15) has a real part which is the speed of propagation of the disturbance and an imaginary part which gives the growth rate. We are interested in the conditions and, in particular, the mean speed of the gas $\langle U_g \rangle$, which gives no growth. The imaginary part of the wave speed vanishes when

$$\frac{\rho_g \langle U_g \rangle^2}{\rho_l g/k + \gamma k} = \frac{1}{\Pi} = \Phi(\text{Re}) = \frac{\text{Re}}{-Q_{gr}P_r + Q_{gi}P_i - 3\Delta Q_{li}},\tag{16}$$

where the final subscripts denote the real and imaginary parts. From our evaluation of the mass fluxes Q_g and ΔQ_l in Sec. VI C and from our evaluation of the pressure normalization constant P in our previous paper[2] (there a factor Re smaller), we can now evaluate $\Phi(\text{Re})$ defined to be the right-hand side of (16). The result is plotted in Fig. 8. For small Reynolds numbers, we found previously[2] (now converted to the viscous scaling of pressure) that $P_r \sim 3i - \frac{54}{35}\text{Re}$, while our numerical test for the meniscus region in Sec. V B gave Q_g and $\Delta Q_l = 1 + O(\text{Re}^2)$ as $\text{Re} \to 0$. Hence $\Phi \sim \frac{35}{54}$. As Re increases, Φ increases, passing through the value 1 by Re $=30$. Also plotted in Fig. 8 is the corresponding result of our first paper,[2] in which we effectively took Q_g and $\Delta Q_l=1$ and so had $\Phi=1/-P_r(\text{Re})$. That previous theory passed through $-P_r=1$ at $\text{Re}=185$. The value $\Phi=1$ is important in that it is the value taken by the original simple theory,[1] which gave a better prediction of their experiments than our "improved" theory[2] incorporating the correct velocity profile across the gap in the outer region.

Equation (16) gives the condition of no growth. We now wish to minimize the mean gas velocity $\langle U_g \rangle$ which satisfies this condition, minimizing over the wavenumber k. There is a slight complication that our calculation of the flow in the inner and outer regions was nondimensionalized using k.
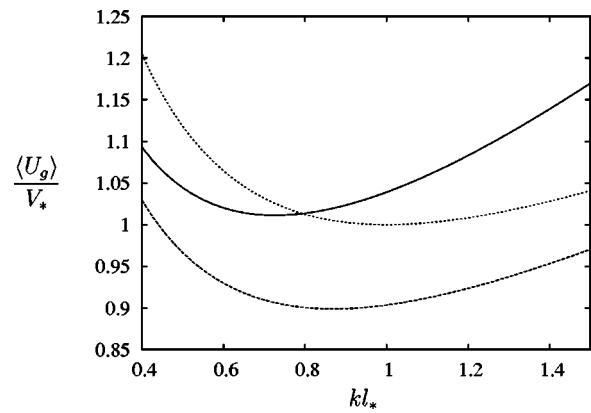
Fortunately with our viscous scaling of the pressure, the wavenumber k only enters our result Φ in the combination of the reduced Reynolds number $\text{Re}=\rho_g \langle U_g \rangle k h^2/\mu_g$. It is convenient to introduce a capillary length scale l_* and the gas velocity V_* whose Bernoulli's pressure has the capillary pressure of this length, along with a reduced Reynolds number Re_* based on these two quantities

$$l_* = \sqrt{\frac{\gamma}{\rho_l g}}, \quad V_* = \sqrt{\frac{2\gamma}{\rho_g l_*}}, \quad \text{Re}_* = \frac{\rho_g V_* h^2}{\mu_g l_*}.\tag{17}$$

With these definitions, Eq. (16) can be rearranged to

$$\left(\frac{\langle U_g \rangle}{V_*}\right)^2 = \frac{1+(kl_*)^2}{2kl_*}\Phi(\text{Re})\tag{18}$$

with

$$\text{Re} = \text{Re}_* \frac{\langle U_g \rangle}{V_*} k l_*.$$

We now plot in Fig. 9 the right-hand side of Eq. (18) as a function of kl_* for $\text{Re}_*=40$. We also plot the corresponding results of our previous theory which used $1/-P_r(\text{Re})$ in place of the $\Phi(\text{Re})$ of this paper, along with the results of the simple Euler–Darcy theory which sets $\Phi=1$. The simple Euler–Darcy theory has a minimum mean gas velocity of $\langle U_g \rangle=V_*$ at $kl_*=1$. Our previous theory gave a minimum velocity of $0.899V_*$ at $kl_*=0.875$ when $\text{Re}_*=40$, while our new theory has a minimum of $1.011V_*$ at $kl_*=0.725$. The simple Euler–Darcy theory takes the destabilizing Bernoulli pressure to be $\rho_g \langle U_g \rangle^2$ independent of the Reynolds number. Our previous theory of the velocity profile across the gap in the outer region found a higher pressure. An increase in the pressure requires a lower mean gas velocity to overcome the stabilizing effects of gravity and surface tension. Our new theory reduces the destabilizing pressure by reducing the flux out of the inner meniscus region into the outer region. As well as the increase in the minimum mean gas velocity, the wavenumber which minimizes the velocity decreases progressively from the Euler–Darcy value $kl_*=1$ to our previous
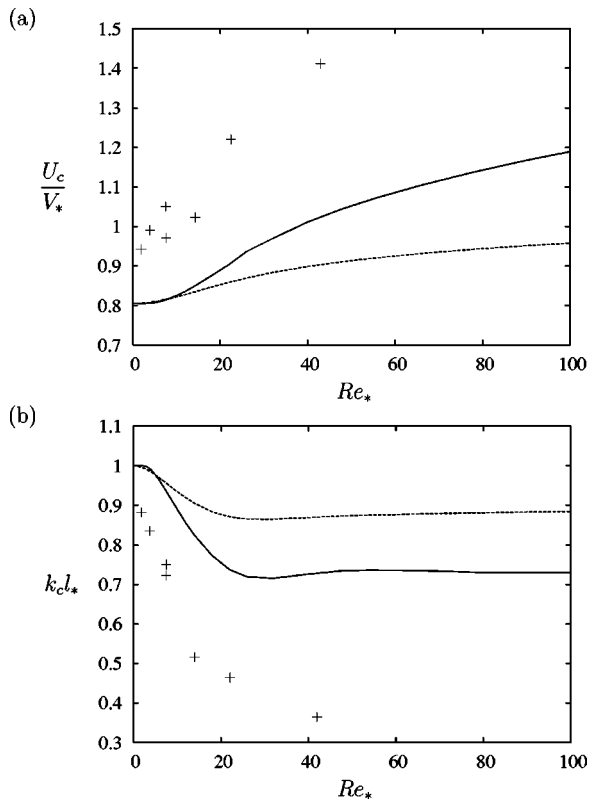
FIG. 10. (a) The minimum mean gas velocity U_c for an instability as a function of the Reynolds number Re$_*$ and (b) the minimizing wavenumber k_c. The continuous curve is our new theory, while the dashed curve is the corresponding results of our previous theory. The points are experimental results (Ref. 3).

theory, to our new theory. These reductions in the wavenumber reflect the reduction of Φ with Re and so k.

Figure 9 is for Re$_*$=40. We have plotted similar figures for a range of Reynolds numbers Re$_*$ and found the minimum U_c mean gas velocity $\langle U_g \rangle$ and minimizing wavenumber k_c in each case. We plot in Fig. 10(a) the minimum value U_c/V_* as a function of Re$_*$, and in Fig. 10(b) the minimizing $k_c l_*$. We also plot the corresponding results for our previous theory. The minimum gas velocity to produce an instability is seen to increase with the Reynolds number Re$_*$. Part of this stabilization is due to a reduction of the destabilizing Bernoulli pressure in the outer region, represented by our pressure coefficient P_r found in our previous paper. But there is a similar magnitude of stabilization caused by the reduced mass flux Q_g, a result of the analysis of this paper. Our new prediction for the minimum gas velocity U_c reaches V_* the value of the simplest Euler–Darcy theory by Re$_*$=39.

VII. COMPARISON WITH EXPERIMENTS

We now compare our new predictions for the onset of the instability with two sets of experimental observations, the original experiments[1] and some later experiments[3] in which the gap width was varied.

Our calculations have been made for a flat interface across the gap with 90° contact angles with the sidewalls. The experiments were, however, performed with perfectly wetting fluids with 0° contact angles and a semicircular in-

terface across the gap. This form of the interface changes two details, first the flow in the meniscus region and second the stabilizing capillary pressure. We have not yet been able to extend our numerical calculation of the flow in the meniscus region to the curved geometry of the semicircular interface, and so our comparison with experiments must be less than satisfactory. The stabilizing capillary pressure, on the other hand, can be corrected by application of the Park and Homsy[4] $\pi/4$ factor, which we will now include.

The original experiments[1] used nitrogen gas of density $\rho_g=1.28$ kg m^{-3} and viscosity $\mu_g=17.5\times10^{-6}$ Pa s with a silicon oil of density $\rho_l=965$ kg m^{-3} and interfacial tension $\gamma=20.6\times10^{-3}$ N m^{-1}. The half-gap thickness was $h=0.175\times10^{-3}$ m and the gravity $g=9.81$ m s^{-2}. Replacing γ by the Park and Homsy corrected value $\gamma(\pi/4)$ in the capillary length and velocity in Eq. (17), we have for these experiments

$$l_* = 1.31 \times 10^{-3} \text{ m}, \quad V_* = 4.40 \text{ m s}^{-1}, \quad R_* = 7.54.$$

At the latter Reynolds number, we now predict the minimum gas velocity for an instability $U_c=0.814V_*$ occurring at a wavenumber $k_c l_*=0.956$. This is hardly any different to our previous predictions $U_c/V_*=0.815$ at $k_c l_*=0.956$. The experiments found $U_c/V_*=1.05$ at $k_c l_*=0.75$. Our new theory therefore fails to make any progress in reducing the disagreement between theory and observations for the first experiments.

In a second series of experiments,[3] the same nitrogen and a slightly different silicon oil of density $\rho_l=952$ kg m^{-3} and interfacial tension $\gamma=20\times10^{-3}$ N m^{-1} were used. These give the capillary length and velocity of Eq. (17)

$$l_* = 1.30 \times 10^{-3} \text{ m}, \quad V_* = 4.35 \text{ m s}^{-1}.$$

Several gap widths were used $2h=0.175$, 0.25, 0.35, 0.48, 0.60, and 0.83 mm. We have plotted the experimental results for the minimum gas velocity for instability and the minimizing wavenumber in Fig. 10. We see that the experimental data are well above the predictions of our first paper and that our new theory is a substantial move in the correct direction but still falls someway short. It may be that using the proper semicircular interface in the calculation of the flow in the inner meniscus region would produce a larger effect.

VIII. MECHANISM

We now give a pictorial account of the Kelvin–Helmholtz instability in a Hele-Shaw cell, see Fig. 11. Because the viscosity of the liquid is much larger than that of the gas, the gas moves rapidly over an effectively static liquid. The liquid responds slowly to the viscous stresses applied by the gas flow. The motion of the liquid gives the propagation and growth of a perturbation of the interface.

Making the gas satisfy the no-slip boundary condition on the perturbed interface induces a perturbation to the downstream gas flow u_{0g} which is negative over the crests (where the mean flow is positive) and positive in the troughs (where the mean flow would be negative), as denoted by the double arrows in Fig. 11(a). The convergence of this flow in the meniscus region to the left of the crests drives a mass flux Q_l
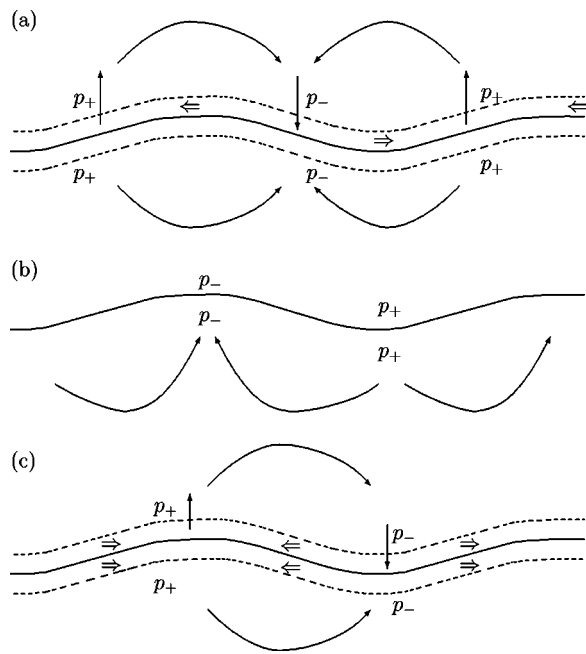
FIG. 11. Physical explanation of the instability. (a) The basic flow viscous flow. (b) Bernoulli suction causes growth. (c) Two small inertial corrections.

there out into the outer region of the gas flow, with a similar divergence to the right of the crests driving a mass flux there into the meniscus region, as denoted by the vertical arrows in Fig. 11(a). In the outer region, the gas flows from the left to the right of the crests, as denoted by the upper curved arrows in Fig. 11(a). Being a Hele-Shaw flow, this flow of the gas requires a positive pressure to the left of the crests and a negative pressure to the right. This pressure distribution $p_g = Q_g P$ is the main part of the viscous stress exerted by the gas on the liquid. The liquid responds with a Hele-Shaw flow from the left to the right of the crests, as denoted by the lower curved arrows in Fig. 11(a). This flow of the liquid raises the interface to the right of the crests and lowers it to the left, i.e., propagates the perturbation to the right.

The paragraph above describes the flow when it is viscously dominated. Inertia must be added to give a growth of the perturbation. Now in the gas outer region, the perturbation to the horizontal flow U_g is in the direction of the mean flow over the crests and against it over the troughs, i.e., taking the mean and perturbation velocities together, the flow speeds up over the crests and slows down over the troughs. To accelerate the flow over the crests an inertial reduction of the pressure is required there, with a corresponding increase over the troughs, as indicated in Fig. 11(b). This distribution of pressure $(Q_g P)_r$ in the gas is applied to the liquid below, and there drives the Hele-Shaw response indicated by the curved arrows in Fig. 11(b). The crests then tend to rise and the troughs descend, for a growth of the perturbation of the interface. This destabilizing Bernoulli suction of the crests upwards has to overcome the stabilizing effects of gravity and surface tension, which sets a minimum gas velocity U_c for an instability.

At low Reynolds numbers Re, the destabilizing Bernoulli pressure takes a (dimensional) value $\frac{54}{35}\rho_g \langle U_g \rangle^2 k \zeta_0$

from $P_r = -\frac{54}{35}$Re and $Q_g = 1$. The approximately parabolic velocity profile across the gap produces the numerical factor $\frac{54}{35}$ increase in the value of the standard not-in-a-Hele-Shaw-cell Kelvin–Helmholtz theory. As the Reynolds number increases, both $-P_r$ and Q_g decrease. We calculated the factor P_r from the outer gas flow in our previous paper. Above Re=10, the velocity profile in the outer gas region has a maximum not in the center of the gap but near the walls. There the mean velocity is slower, giving longer for a smaller pressure gradient to accelerate the prescribed mass flux. In this paper, we calculated the mass flux Q_g of gas out of the meniscus region into the gas outer region, and found that its real part decreases with Re. This reduction comes from the downstream velocity perturbation u_{0g} having less time, when the mean flow $\langle U_g \rangle$ is faster at higher Re, to react to the perturbations of alternating signs diffusing from the interface.

While inertia is responsible for the destabilizing Bernoulli suction over the crests, it also gives two small corrections, one stabilizing and the other destabilizing. Within the gas meniscus region, strong advection by the mean flow leads to the maximum of the downstream velocity perturbation not being in the trough as in Fig. 11(a) but being a little downstream of the trough, with the minimum similarly being a little downstream of the crests. This out-of-phase $u_{goi} > 0$ is denoted by the upper double arrows in Fig. 11(c). The convergence and divergence of this meniscus flow leads to the out-of-phase mass flux $Q_{gi} < 0$, denoted by the vertical arrows in Fig. 11(c). The Hele-Shaw flow in the gas outer region requires a pressure maximum on the crests and a minimum in the troughs. Exerting this pressure on the gas drives a liquid flow which raises the troughs and pushes down the crests, i.e., is a stabilizing effect. The downstream velocity perturbation in the gas meniscus region also exerts a viscous stress on the liquid, driving an out-of-phase liquid flow $u_{loi} > 0$ denoted by the lower double arrows in Fig. 11(c). The convergence and divergence of this liquid flow produces the extra mass flux $\Delta Q_{li} < 0$, which pushes up the interface in the crest and pulls it down in the trough, i.e., is a destabilizing effect. Both these effects are small numerically.

IX. CONCLUSION

We have found that the small meniscus region within a gap width of the interface has a large $O(1)$ effect on the Kelvin–Helmholtz instability in a Hele-Shaw cell. Normally one would expect to ignore this small region, just calculating what are our outer flows either side of the interface and to them then applying dynamic and kinematic boundary conditions across the interface. From Park and Homsy,[4] we have known for some time that the curved interface enhances the capillary pressure in the dynamic boundary condition by the factor $\pi/4$ for a perfectly wetting liquid. The unexpected result of this paper is that the kinematic boundary condition must also be modified in some studies. One cannot apply a mass conservation condition to the outer flows

$$\frac{\partial \zeta}{\partial t} + \bar{u}\frac{\partial \zeta}{\partial x} = \bar{w},$$

where the overbar denotes an average taken across the width of the gap. The above equation would say $Q_g = 1$, which we have found to be true only at small Reynolds numbers Re.

The reason the small region has a large effect is that the downstream velocity is very much larger in the meniscus regions compare with that in the outer regions. The outer regions have horizontal and vertical length scales both equal to the wavelength. Mass conservation then gives the horizontal and vertical velocities must be the same size in the outer regions. The vertical velocity has the same size in the outer as in the inner meniscus region. The horizontal velocity in the meniscus region is then necessarily larger than vertical velocity by the ratio of the wavelength to the vertical extent of the meniscus region, the width of the gap. Thus the horizontal velocity is an order of magnitude larger in the meniscus region compared with the outer. Variations over a wavelength of this large velocity in the small region produces the $O(1)$ mass flux Q_g seen by the outer. Inertia reduces the value of Q_g when $\mathrm{Re} > 0$.

Despite the radical change from our previous paper in the predictions for the minimum gas velocity for an instability, we have not yet successfully predicted the values observed in experiments. The numerical calculations in this paper have, for considerable convenience, been made with a flat interface across the gap with 90° contact angles. An accurate calculation with the correct semicircular interface for a perfectly wetting liquid would be very demanding, but would certainly yield further $O(1)$ changes in the predictions. There are other simplifications of the experiments made by the theory which we detailed in our previous paper.[2] Perhaps problems of the moving contact line remain the source of the largest uncertainty.

In this paper, we have concentrated on the minimum gas velocity for an instability. Experiments have examined a number of other features, such as the phase velocity and spatial growth rates.[1,3] Subcritical nonlinear behavior has been reported.[5] Our opinion is that a careful analysis of these behaviors cannot be contemplated before the onset condition can first be successfully predicted, and that may require mastering the effects of the moving contact line.

[1]P. Gondret and M. Rabaud, "Shear instability of two-fluid parallel flow in a Hele-Shaw cell," Phys. Fluids **9**, 3267 (1997).

[2]P. Plouraboué and E. J. Hinch, "Kelvin–Helmholtz instability in a Hele-Shaw cell," Phys. Fluids **14**, 922 (2002).

[3]L. Meignin, P. Ern, P. Gondret, and M. Rabaud, "Gap size effects for the Kelvin–Helmholtz instability in a Hele-Shaw cell," Phys. Rev. E **64**, 026308 (2001).

[4]C.-W. Park and G. M. Homsy, "Two-phase displacement in Hele-Shaw cells: Theory," J. Fluid Mech. **139**, 291 (1984).

[5]L. Meignin, P. Gondret, C. Ruyer-Quil, and M. Rabaud, "Subcritical Kelvin–Helmholtz instability in a Hele-Shaw cell," Phys. Rev. Lett. **90**, 234502 (2003).